Applied Catalysis A: General 530 (2017) 21–29

Contents lists available at ScienceDirect

Applied Catalysis A: General

journal homepage: www.elsevier.com/locate/apcata

Performance of co-doped Mn-Ce catalysts supported on cordierite for low concentration chlorobenzene oxidation

Jiawei Kan[a,b], Lei Deng[a,b], Bing Li[a,b], Qiong Huang[d], Shemin Zhu[a,c], Shubao Shen[a,b], Yingwen Chen[a,b,*]

[a] State Key Laboratory of Materials-Oriented Chemical Engineering, Nanjing Tech University, Nanjing 210009, China
[b] College of Biotechnology and Pharmaceutical Engineering, Nanjing Tech University, Nanjing 210009, China
[c] College of Materials Science and Engineering, Nanjing Tech University, Nanjing 210009, China
[d] Jiangsu Engineering Technology Research Center of Environmental Cleaning Materials, Nanjing University of Information Science and Technology, Nanjing 210044, China

ARTICLE INFO

Article history:
Received 29 August 2016
Received in revised form 3 November 2016
Accepted 10 November 2016
Available online 11 November 2016

Keywords:
Chlorobenzene
Mn-Ce/cordierite catalysts
Mn-Co-Ce/cordierite catalysts
Synergistic effect
Lattice defect

ABSTRACT

The catalytic activity for low concentration chlorobenzene oxidation was measured with Mn-Ce/cordierite and Mn-Co-Ce/cordierite catalysts with different mole ratios, which were prepared by a sol-gel method and characterized using XRD, BET, SEM Raman, H_2-TPR and XPS. The results demonstrated that part of the manganese and cobalt could be incorporated into the lattice of CeO_2 to form a solid solution phase. Among all of the catalysts synthesized, $Mn_8Co_1Ce_1$/cordierite presented the best activity and stability. When the concentration of chlorobenzene was 500 ppm, and the GHSV was 15000 h^{-1}, the complete combustion temperature ($T_{90\%}$) of chlorobenzene was 325 °C. In addition, there was almost no change in the conversion of chlorobenzene during the long-term reaction at 350 °C. These results were primarily attributed to the synergistic effect of ceria, manganese and cobalt, which can promote the formation of more lattice defects, more oxygen vacancies and smaller crystallite sizes.

1. Introduction

In recent years, volatile organic compounds (VOCs) have attracted considerable attention because they contribute the most to air pollution, such as chemical smog and atmospheric haze, which seriously affects the environment and the health of people. Chlorinated volatile organic compounds (CVOCs), a type of VOCs, are a special group due to their acute toxicity and persistency; they are released to the atmosphere from the petrochemical, medical, mechanical and painting industries [1,2]. Compared with other VOC elimination techniques, catalytic combustion has been considered as a promising technology owing to its high conversion efficiency (at temperatures between 250 and 550 °C) and especially its limited secondary pollution and low energy consumption compared to thermal combustion [3,4]. Chlorobenzene (CB) is a chlorinated contaminant from industrial processes that is frequently used as the model for CVOCs because it is a precursor or intermediate product of polychlorinated wastes, such as PCDD/PCDF [5,6].

Generally, there are three categories of catalysts used for the oxidation of CVOCs: noble metals [7–9], transition metals [10–12] and zeolites [13–15]. Although noble metal catalysts show higher activity, they are unable to resist chlorine poisoning during the catalytic combustion process [16,17]. Moreover, the high value and low reserves of precious metal elements can limit their practical application. The high activity that zeolites present is attributed to their acidic properties; however, this catalyst system would generate polychlorinated by-products that would result in secondary pollution. Compared with the above-mentioned catalysts, transition metal oxides have better thermal stability, a strong toxic resistance and low cost, and they have been explored and used extensively [18]. Among transition metals, Ce-containing transition metal composite oxides have been considered as potential catalysts for CB oxidation due to their high oxygen storage capacity, abundant oxygen vacancies and strong redox property from the valence change of Ce^{3+}/Ce^{+4} [19,20]. However, the active sites of CeO_2-based catalysts are easily occupied due to the strong adsorption of HCl or Cl_2 produced from the degradation of CB. Despite the poor stability, some Ce-containing composite oxides have been explored by many researchers, and some of these composite oxides showed

* Corresponding author at: State Key Laboratory of Materials–Oriented Chemical Engineering, College of Biotechnology and Pharmaceutical Engineering, Nanjing Tech University, No. 5 XinMoFan Road, Nanjing 210009, China.
E-mail address: ywchen@njtech.edu.cn (Y. Chen).

http://dx.doi.org/10.1016/j.apcata.2016.11.013
0926-860X/

higher catalytic efficiency and stability, such as Mn-Ce [21], V-Ce [5] and Cr-Ce [22] catalysts. Moreover, Chen et al. [23] discussed that the Co-Cu-Mn mixed-oxide catalyst exhibited high catalytic activity in the oxidation of VOC binary mixtures and single components, and the catalyst showed excellent stability during the 550 h long-term reaction. The Co_3O_4/La-CeO_2 catalyst was found to provide more adsorbed species and lattice oxygen species in the combustion of toluene and a mixture of toluene and dioxygen due to the interaction between the Co^{3+}/Co^{2+} and Ce^{4+}/Ce^{3+} couples, which resulted in an enhancement of the catalytic activity and the reaction rate [24]. He et al. [25] reported that the nanostructured mesoporous CuO-MnO_x-CeO_2 catalyst with a Cu/Mn atomic ratio of 1/1 presented the best catalytic efficiency of CB by providing of large amounts of oxygen vacancies. However, the active component Co-doped Mn-Ce for the catalytic combustion of CB was not discussed. Meanwhile, the radius of Co^{3+} is between that of Mn^{3+} and Ce^{4+}, which could lead to the formation of a ternary solid solution catalyst. The doping of Co ions probably promotes the formation of more lattice defects and oxygen vacancies and improves the oxygen mobility. Therefore, Co-doped Mn-Ce/cordierite catalysts may exhibit a high catalytic activity for chlorobenzene oxidation and remove the Cl adsorbed on the surface of the catalysts. To enable the industrial use and practical application of catalysts for removing CB, supported non-noble catalysts, especially the Mn-Co-Ce catalysts, should be investigated. Among a variety of catalyst supports, cordierite is usually recognized as an excellent carrier by virtue of its pore structure and high temperature resistance; however, it is has seldom been reported as a catalyst support for the catalytic combustion of CB. Hence, Co-doped Mn-Ce/cordierite catalysts are worth researching in the catalytic combustion of chlorobenzene.

Consequently, the Co-doped Mn-Ce mixed-oxide catalysts supported on cordierite with different molar ratios of Mn-Ce and Co-Mn-Ce were synthesized through the sol-gel method and were tested in the catalytic combustion of low concentration CB. Characterization of the supported catalysts was performed by XRD, BET, SEM, Raman, H_2-TPR and XPS.

2. Experimental procedures

2.1. Catalyst preparation

The cordierite support was modified by our team by boiling in 10 wt% nitric acid for 2 h, and then, it was dried at 80 °C for 2 h and finally calcined under air atmosphere at 500 °C for 2 h [26].

The Co-doped Mn-Ce catalysts supported on cordierite were manufactured using a sol-gel method, as follows: an aqueous solution containing $Ce(NO_3)_3{\cdot}6H_2O$ (SCRC, 99%), $Mn(NO_3)_2$ (50 wt% solution), $Co(NO_3)_2{\cdot}6H_2O$ (SCRC, 99%) and citric acid (SCRC, 99%, n(citric acid): n(Ce + Mn + Co) = 1:6) was gradually heated to 60 °C, and then 4 g of pretreated cordierite was dipped into that solution and subsequently maintained at that temperature for 5 h under continuous stirring to produce a sol. After the sol was aged for 12 h, the compound was dried overnight at 110 °C and then calcined in air at 500 °C for 5 h. Catalysts with 20 ± 1% loading were obtained, which included different atomic ratios (Mn: Co: Ce = 3:1:1, 8:1:1 and 2:2:1) based on the Mn-Ce/cordierite catalyst that was prepared by the same method (Mn: Ce = 1:1, 2:1, 4:1). To increase the readability, *x*, *y* and 1 in $Mn_xCo_yCe_1$/cordierite represent the molar ratios of Mn, Co and Ce, respectively, in this paper.

2.2. Catalyst characterization

Powder X-ray diffraction (XRD) patterns were recorded on an AXS D8 advance diffractometer equipped with a graphite monochromator and Cu-Ka radiation in the 2θ range from 5–80° with a scanning rate of 5°/min. The nitrogen adsorption and desorption isotherms were measured at −196.8 °C on a Tristar3020 M Micromeritics apparatus. The samples were treated in vacuum at 80 °C for 8 h before the measurements. The specific surface area was calculated using the BET model, and the pore size distribution and average pore diameter were derived from the desorption branch of the N_2 isotherm using the Barrett-Joyner-Halenda (BJH) method. Scanning electron microscopy (SEM) images were obtained on a JSM-5900 instrument after the samples were pre-coated with gold. Raman spectra were obtained on a DXR532 spectrometer at ambient temperature and under moisture-free conditions. Raman signals were produced with the 532 nm emission line from an Ar+ ion laser and a spot size of approximately 1 mm. The acquisition time was varied according to the intensity of the Raman scattering, and the wavenumbers obtained from the spectra were accurate to within 0.1 cm^{-1}. The H_2-temperature programmed reduction (H_2-TPR) experiments were performed on an automated chemisorption analyzer (Quantachrome Instruments) using 100 mg of the catalyst under flowing (70 mL/min) hydrogen (10 vol.%) and nitrogen (90 vol.%). The temperature of the catalysts was increased at a rate of 10 °C/min. A thermal conductivity detector was used to monitor the hydrogen consumed during the TPR experiment. Before the analysis, the sample was purged with helium (70 mL/min) at 50 °C for 0.5 h. The X-ray photoelectron spectroscopy (XPS) measurements were performed using a PHI-5000C ESCA system (PerkinElmer) with Mg-Ka radiation (hv = 1253.6 eV) or Al-Ka radiation (hv = 1486.6 eV) as the excitation source. In general, the X-ray anode was operated at 250 W, and a high voltage was maintained at 14.0 kV with a detection angle of 54○. The sample was pressed directly into a self-supported disk (10 × 10 mm), mounted on a sample holder, and then transferred into the analysis chamber.

2.3. Evaluation of catalytic activity

CB oxidation was carried out in a fixed-bed flow reactor with a quartz tube with an inner diameter of 10 mm under atmospheric pressure. Two grams of the catalyst was placed in the middle of a quartz reactor erected in the center of a tubular furnace. The CB stream was fed into the reaction system by bubbling air into the liquid CB solution at 55 °C, and then it was mixed with another air stream. To precisely simulate the relatively low concentration of CVOCs from industrial processes, the feed flow through the reactor was set with a CB concentration of 500 ppm and a gas hourly space velocity (GHSV) of 15000 h^{-1} [27]. The reaction temperature was controlled with a thermocouple in the range of 150–400 °C. In addition, the pipeline was heated to 55 °C and kept at that temperature to decrease the condensation and adsorption of CB on the inner surface. The inlet and outlet gases were analyzed after stepwise changes in the reaction temperature using an on-line gas chromatograph (GC2014, Shimadzu Corp) equipped with a FID detector and a Restek RTX-1 column for the quantitative analysis of CB. The quality of CO and CO_2 was analyzed by the on-line gas chromatograph (GC2014, Shimadzu Corp) with a TCD detector. In addition, no organic polychlorinated benzene was produced during the catalytic combustion of CB, according to the observation of the outlet chromatographic peak that only displayed the CB peak. The concentration of both HCl and Cl_2 was measured by bubbling the exhaust gases through a 0.0125 mol·L^{-1} NaOH solution. The Cl_2 concentration in the bubbled solution was determined by chemical titration with ferrous ammonium sulfate (FAS) using N,N-diethyl-*p*-phenylenediamine (DPD) as the indicator [28], and the Cl^{-1} concentration was tested by using an ion-selective

electrode [29]. The catalytic activity of CB and the CO_2 selectivity are calculated by the following equations:

$$\eta_1 = \frac{C_1 Q_{sn1} - C_2 Q_{sn2}}{C_1 Q_{sn1}} \times 100\% \quad (a)$$

where η_1 is the conversion efficiency, C_1 and C_2 (mg/m^3) are the inlet and outlet concentrations of chlorobenzene and Q_{sn1} and Q_{sn2} (m^3/h) are the inlet and outlet fluxes of air, respectively.

$$S_{CO_2} = \frac{n_{CO_2}}{(6 \cdot n_{CB})} \times 100\% \quad (b)$$

where n_{CO_2} and n_{CB} are moles of CO_2 produced in the outlet gas and the moles of CB feed in the inlet gas, respectively.

3. Results and discussion

3.1. Catalytic activity for CB combustion

The conversion of CB over different types of supported catalysts synthesized is presented in Fig. 1. As shown in Fig. 1, the $Mn_8Co_1Ce_1$/cordierite catalyst exhibited the best activity under the same reaction conditions, and almost 90% conversion of CB was obtained when the temperature reached 325 °C. Compared with the $T_{90\%}$ (the temperature at which a 90% conversion is attained) of the other catalysts, it appears that the efficiency of all supported catalysts were as follows: $Mn_8Co_1Ce_1$/cordierite > $Mn_3Co_1Ce_1$/cordierite > $Mn_2Co_2Ce_1$/cordierite > Mn_4Ce_1/cordierite > Mn_2Ce_1/cordierite > Mn_1Ce_1/cordierite. The performance of the representative Ce-based catalysts has been investigated for the CB oxidation. MnO_x-CeO_2 [21], MnO_x/CeO_2-NPS [30], CuO/CeO_2 [31] and Mn-Ce-Mg/Al_2O_3 [32] have been investigated for the catalytic combustion of CVOCs. Ma et al. [31] reported that mesoporous CuO/CeO_2 bimetal oxides were very active for the catalytic destruction of 1,2-dichlorobenzene. Wu et al. [32] showed that Mn-Ce-Mg/Al_2O_3 catalysts exhibited high activity, good selectivity and desired stability for the catalytic oxidation of chlorobenzene. It is well known that the unsupported catalysts are unsuitable for practical applications because of their high cost and low service life. However, the system of Mn-Ce catalysts supported on cordierite has rarely been studied; in addition, it did not show better activity than the aforementioned unsupported catalysts, and the CB conversion is less than 90% at 350 °C over the Mn_4Ce_1/cordierite catalyst presented in this paper. It can be observed in Fig. 1 that Mn_4Ce_1/cordierite presents a higher catalytic activity than the other two catalysts, and more than 90% of the CB is not converted until 375 °C. The results in this paper indicate that the activity of the catalyst is significantly improved with the addition of a small amount of Co [33–35]. Therefore, $Mn_8Co_1Ce_1$/cordierite is a promising ternary oxide catalyst for CB treatment.

The oxidation mechanism of chlorobenzene over Mn-Ce/H-ZSM5 and V_2O_5/TiO_2 catalysts has been studied by Sun et al. [36] and Lichtenberger et al. [37], and the researchers proposed that the nucleophilic and electrophilic substitutions occurred towards CB combustion. It is known that the energy of C—Cl bonds is weaker than that of C—H bonds, and therefore, the C—Cl bonds are more likely to be attacked by nucleophiles. First, dissociative adsorption on the active cobalt and manganese sites occurred via Cl abstraction in the molecular combustion of chlorobenzene. The dissociated Cl was absorbed over the surface of the Mn_4Ce_1/cordierite and $Mn_8Co_1Ce_1$/cordierite catalysts. At low reaction temperatures (<200 °C), chlorobenzene adsorption was the main control step, and the adsorbed Cl could not be removed until the dynamic equilibrium of adsorbed and desorbed Cl species was achieved due to the absence of active oxygen species or the synergistic effect of cobalt, manganese and cerium, which was clarified by XPS. In the process above, the partial desorption of Cl may lead to the formation of a small amount of organic byproducts, and then the organic byproducts are further oxidized by the active oxygen species to produce CO_2, H_2O and HCl. A small amount of HCl may be attached to the surface of the catalysts, and through this, some active sites may be occupied. As the reaction temperature increased, the adsorbed Cl could be removed by the combination of the Deacon Reaction ($4HCl + O_2 \rightarrow 2Cl_2 + 2H_2O$) and active oxygen species. Finally, the consumed oxygen species were replenished by the gas-phase oxygen adsorbed on the oxygen vacancies. This cycle of oxygen species was critical for the rapid elimination of Cl on the active sites.

3.2. Analysis of the products

With regards to FID/TCD detection, the Mn-Ce/cordierite and Mn-Co-Ce/cordierite catalysts presented no polychlorinated byproducts and a selectivity of at least 99.6% to carbon oxides (more than 99% to CO_2 and trace CO). Moreover, the amount of the Cl element of the outlet stream was 12%–15% lower than that of the inlet stream, and the selectivity to the Cl_2 produced during the catalytic combustion of CB was less than 2%; the results indicated that a small amount of chlorinated metals was formed on the surface of the catalysts.

3.3. Long-term reaction of the catalysts

For dealing with CVOCs produced by catalytic combustion from industrial processes, most catalysts were easily poisoned because chlorine typically occupied the active sites through adsorption on the surface of the catalysts [38]. To enable the commercial use of the supported catalysts, the stability of the catalysts is a critical factor. Li et al. [39] tested the stability of Mn-Ti catalysts with different additives for chlorobenzene combustion during a long-term reaction of 30 h, and the Sn-Mn-Ti catalyst showed better stability. Ma et al. [40] examined the stability of CrO_x/Al_2O_3 catalysts for dichloromethane oxidation, which was measured at 300 °C during a long-term reaction of 16 h. Therefore, Fig. 2 presents the results of the stability test at 350 °C for CB combustion, and the variation in activity was observed for 24 h at that temperature. As shown in Fig. 2, the Mn_4Ce_1/cordierite catalyst presented only a 86% initial conversion of CB, and the conversion tended to reduce during the 24 h reaction at 350 °C, decreasing from 86% to 82% in the continuous stream. At the same temperature, all the Mn-Co-Ce/cordierite catalysts exhibited a catalytic efficiency of more than 90% for the catalytic combustion of CB. Comparing the durability of the four catalysts, the downward trend in the activity of the Mn-Co-Ce/cordierite catalysts was smoother than that of the Mn_4Ce_1/cordierite catalyst, which indicated that the addition of cobalt to Mn-Ce/cordierite enhanced the chlorine tolerance owing to the increased mobility of active oxygen species on the surface, which was shown in Section 3.6. In addition, the $Mn_8Co_1Ce_1$/cordierite catalyst showed the initial activity and the best resistance to chlorine poisoning, without a noticeable deactivation during the entire testing phase. The stability of the Mn-Co-Ce/cordierite catalysts decreased as the amount of cobalt ions increased. Therefore, the $Mn_8Co_1Ce_1$/cordierite catalyst was the optimal three-component solid solution in the Mn-Co-Ce/cordierite catalyst system for CB combustion.

3.4. XRD analysis

XRD patterns of the Mn-Ce/cordierite and Mn-Co-Ce/cordierite catalysts are displayed in Fig. 3. From the XRD spectrum, it is observed that the diffraction peak corresponding to the cordierite support is relatively strong because of its high content. Therefore, the relatively weak diffraction peaks of the active components are observed in Fig. 3. According to the XRD profiles in Fig. 3(A), the

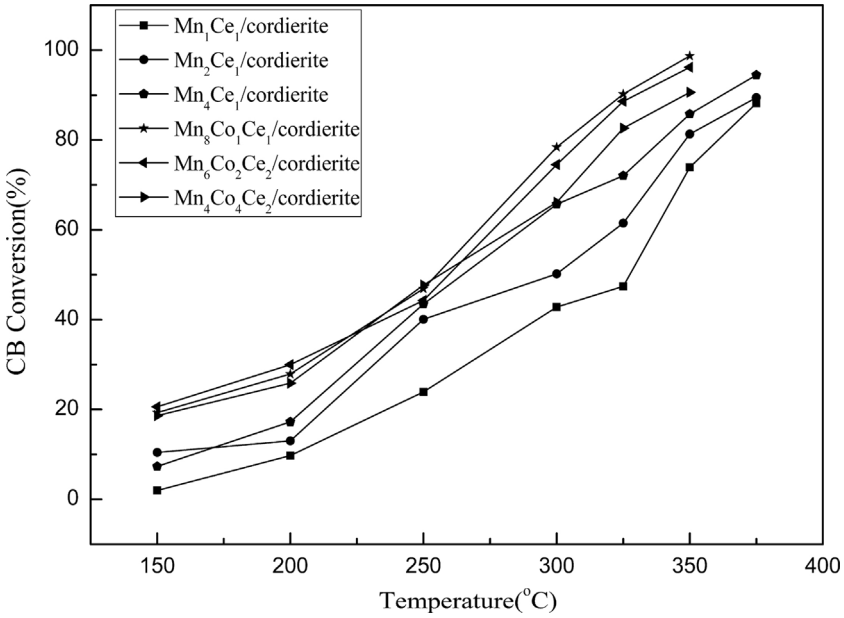

Fig. 1. Catalytic activity for chlorobenzene destruction over the catalysts; the concentration of chlorobenzene: 500 ppm, GHSV = 15000 h^{-1}.

diffraction peaks (at 28.4, 33.0, 47.4 and 56.2°) of CeO_2 with a cubic fluorite-like structure appeared over the Mn-Ce/cordierite catalysts, but these peak positions shifted to the left compared to the standard peak (JCPDS No. 81-0792) [25], and the peak intensity changed slightly as the amount of Mn increased. It is speculated that the crystal lattice of CeO_2 is distorted by the effect of ion doping, and the Ce species with a low content are uniformly distributed on cordierite. For all catalysts with different contents of manganese, no diffraction peak corresponding to manganese oxides are observed, which indicates that the manganese element may be incorporated into the fluorite lattice to form the solid solution since the ionic radius of Mn^{3+} (0.066 nm) is smaller than that of Ce^{4+} (0.094 nm), or it may scatter homogeneously on the surface of CeO_2 [41]. For the Mn-Co-Ce/cordierite catalysts, some diffraction peaks of Co_3O_4 crystallites at 19.0, 36.8 and 68.6° are observed in Fig. 3(B), and the diffraction peak intensity of CeO_2, especially that at 33.0°, clearly decreased. This phenomenon implies that CeO_2 may be covered with highly dispersed cobalt oxides, or part of the cobalt ions also enter into the crystal lattice of CeO_2 to form a ternary solid solution [12]. Subsequently, the Mn-Ce/cordierite modified by the doping of a small amount of cobalt was beneficial to catalytic combustion of CB due to synergistic effects including the variable valence, the oxygen transfer rate and the presence of more active sites. The diffraction peaks of $Mn_8Co_1Ce_1$/cordierite had the broadest of full width at half maximum, especially at 36.8°, which indicated the formation of more lattice defects and a smaller crystallite size [20].

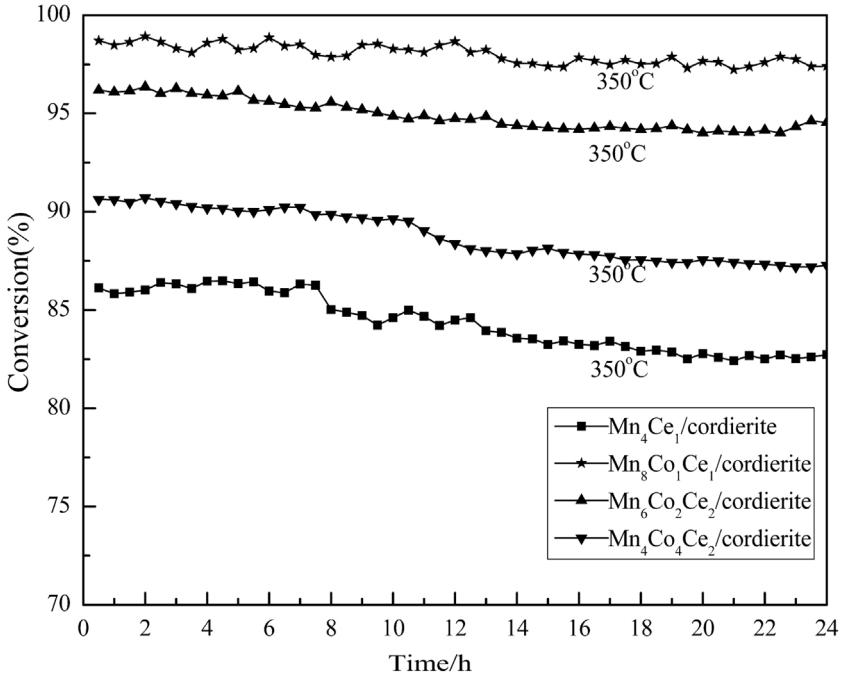

Fig. 2. The stability tests of the Mn-Co-Ce/cordierite catalysts and the Mn_4Ce_1/cordierite catalyst for chlorobenzene oxidation during a sustained reaction of 24 h.

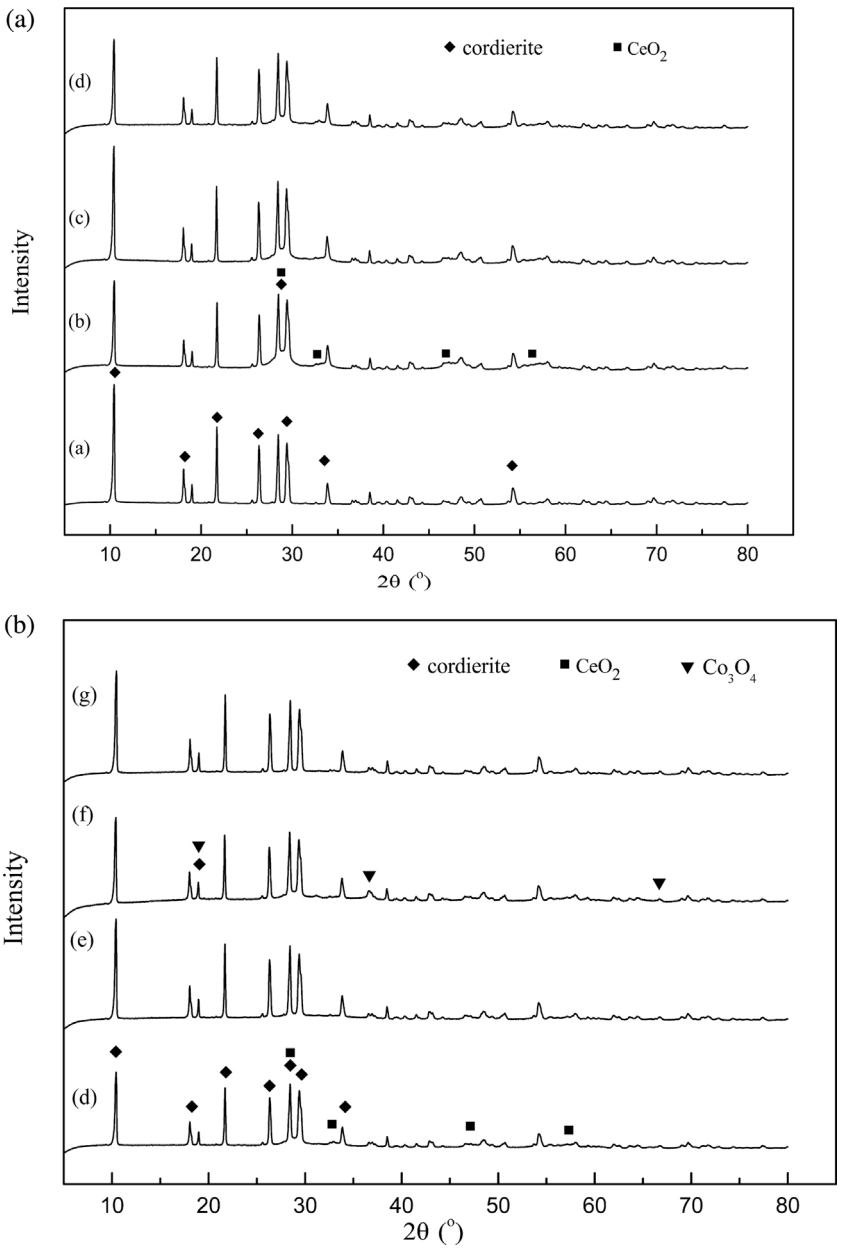

Fig. 3. (A) XRD patterns of the Mn-Ce/cordierite catalysts and cordierite (a: cordierite, b: Mn:Ce = 1, c: Mn:Ce = 2, and d: Mn:Ce = 1) (B) XRD patterns of the Mn-Co-Ce/cordierite catalysts and the Mn_4Ce_1/cordierite catalyst. (d: Mn:Ce = 4 e: Mn:Co:Ce = 3:1:1, f: Mn:Co:Ce = 2:2:1, and g: Mn:Co:Ce = 8:1:1).

Meanwhile, the $Mn_8Co_1Ce_1$/cordierite catalyst showed the superior catalytic performance for chlorobenzene combustion, which was in full accordance with the results above of the catalytic activity.

3.5. N_2 adsorption/desorption

Table 1 lists the specific surface area (S_{BET}), total pore volume (D_V), and average pore size (D_P) of the cordierite and synthetic supported catalysts. The surface areas of all catalysts were much higher than that of pure cordierite (5.0 m^2/g). The S_{BET} value of the Mn-Ce/cordierite catalyst increased with the increase in the manganese content, which indicated that incorporation of a large amount of MnO_x into CeO_2 could promote the dispersion of the catalyst, to some extent. Regardless of if cobalt ions partially replace manganese or cerium ions, after a comparison of the two catalyst systems in Table 1, the S_{BET} of the Mn-Co-Ce/cordierite catalysts decreased slightly compared with that of the Mn_4Ce_1/cordierite catalyst. For chlorobenzene oxidation, although the Cl species from chlorobenzene were easily absorbed on the surface of the catalysts, they could be rapidly removed by catalysts with a large amount of active surface oxygen. Consequently, this did not mean that the catalyst with the largest surface area had the highest catalytic activity.

Table 1
Textural properties of the Mn-Ce/cordierite and Mn-Co-Ce/cordierite catalysts with different molar ratios.

Catalysts	S_{BET} (m^2/g)	D_V (cm^3/g)	D_P (nm)
cordierite	5.0	0.005	3.4
Mn_1Ce_1/cordierite	15.0	0.043	11.6
Mn_2Ce_1/cordierite	16.1	0.052	12.9
Mn_4Ce_1/cordierite	20.4	0.073	14.3
$Mn_3Co_1Ce_1$/cordierite	14.6	0.035	9.6
$Mn_2Co_2Ce_1$/cordierite	16.9	0.042	10.1
$Mn_8Co_1Ce_1$/cordierite	17.0	0.040	9.4

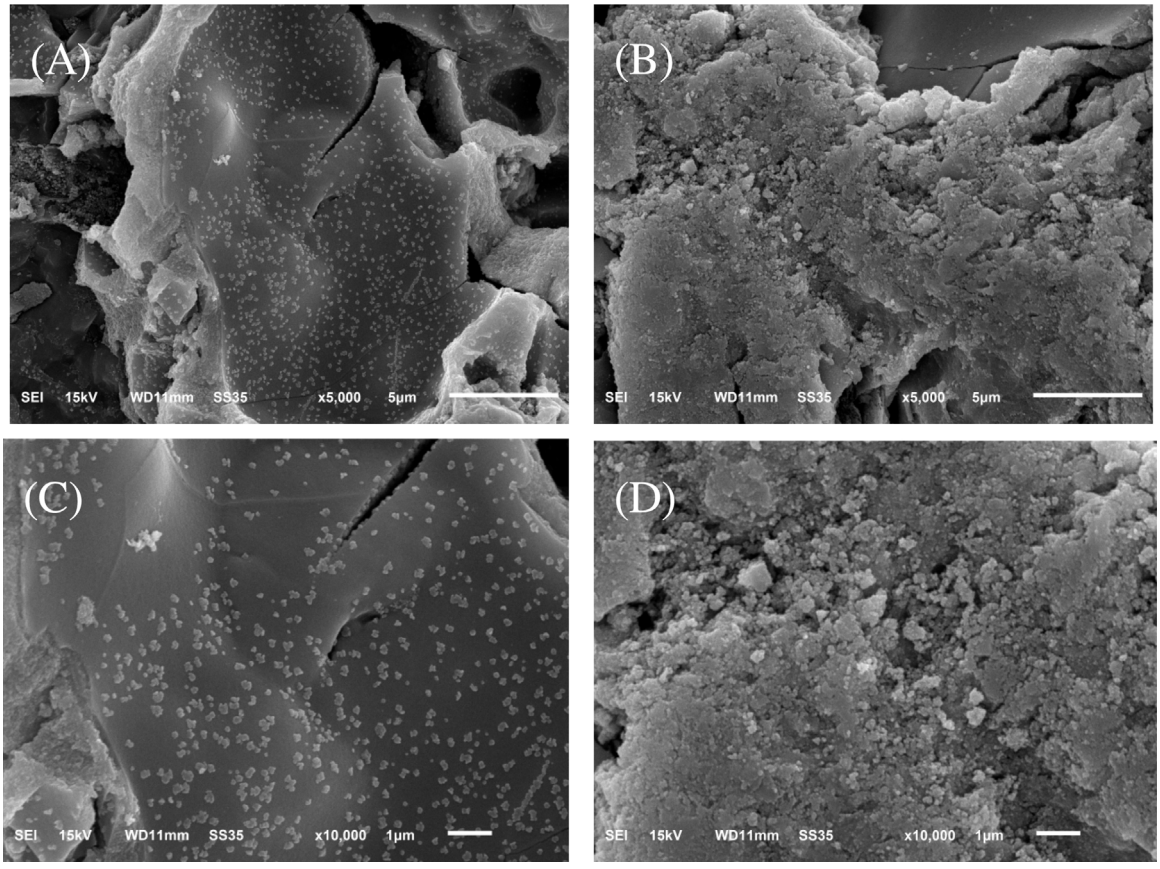

Fig. 4. SEM images of the $Mn_8Co_1Ce_1$/cordierite and Mn_4Ce_1/cordierite catalysts (A, C: $Mn_8Co_1Ce_1$/cordierite, B, D: Mn_4Ce_1/cordierite).

The $Mn_8Co_1Ce_1$/cordierite catalyst had a relatively large specific surface area, which resulted in a high catalytic efficiency in the degradation of chlorobenzene, as shown in Fig. 1.

3.6. Scanning electron microscopy

The surface morphological properties of the Mn_4Ce_1/cordierite and $Mn_8Co_1Ce_1$/cordierite catalysts were investigated by SEM, as shown in Fig. 4. From Fig. 4, it can be observed that the catalysts have morphological structures that are ball-like nanoclusters with asymmetrical sizes. However, the $Mn_8Co_1Ce_1$/cordierite catalyst exhibited a smaller average pore size than the Mn_4Ce_1/cordierite catalyst. As observed in the SEM images, the cordierite was homogeneously covered with active components in Fig. 4(A, C), which indicated that the cobalt dopant can increase the dispersion of the catalyst and prevent the aggregation of manganese and cerium metal particles. The differences above indirectly reflect the synergistic effect of Mn, Co and Ce, which was proposed in Section 3.4.

3.7. Raman spectra

The Raman spectra of the CeO_2/cordierite, Mn_4Ce_1/cordierite and Mn-Co-Ce/cordierite catalysts are shown in Fig. 5. As observed in Fig. 5, the Raman spectra of the CeO_2/cordierite catalyst has a principal peak at 455 cm^{-1} and a weak peak at 252 cm^{-1}, which may be attributed to the strong F_{2g} mode of the fluorite phase and the second-order transverse acoustic mode, respectively [42]. On the other hand, the Mn_4Ce_1/cordierite and Mn-Co-Ce/cordierite catalysts exhibited a single peak at ~430–435 cm^{-1} that shifted to a lower wavelength compared with the F_{2g} band of the CeO_2/cordierite catalyst due to the formation of the Mn-Ce-O and Mn-Co-Ce solid solutions, oxygen vacancies and lattice defects. Moreover, the significant peak offset of the $Mn_8Co_1Ce_1$/cordierite catalyst indicates the formation of more lattice defects in this catalyst. In addition, the amount of oxygen vacancies over the Mn_4Ce_1/cordierite and Mn-Co-Ce/cordierite catalysts was evaluated by a Gaussian deconvolution of the region at approximately 435 cm^{-1} [43]. It can be observed that the $Mn_8Co_1Ce_1$/cordierite catalyst presented the highest vacancy concentration.

3.8. H_2-TPR analysis

The H_2-TPR data for the Mn_4Ce_1/cordierite and Mn-Co-Ce/cordierite catalysts are shown in Fig. 6. The Mn_4Ce_1/cordierite catalyst exhibits three strong reduction peaks at approximately 363, 444 and 591 °C. The first two peaks are associated with a two-step reduction of MnO_2 and Mn_2O_3, respectively [44,45]. The third peak is related to the reduction of the surface Ce^{+4} ions [46]. With regards to the reduction peak area corresponding to Mn species of the Mn-Co-Ce system, the area of the $Mn_8Co_1Ce_1$/cordierite catalyst was larger than that of others, which indicated that more H_2 consumption on the $Mn_8Co_1Ce_1$/cordierite catalyst was required; this demonstrated that the active component has a smaller size and higher dispersion. Compared with the reduction features of the Mn_4Ce_1/cordierite catalyst, the reduction temperatures of the Mn-Co-Ce/cordierite composite metal oxides shifted to lower temperatures in the temperature range of 300–450 °C, and the offset increased as the doping amount of cobalt increased. For the $Mn_2Co_2Ce_1$/cordierite (reduction peaks at approximately 330, 390 and 566 °C) and $Mn_3Co_1Ce_1$/cordierite catalysts (reduction peaks at approximately 352, 400 and 570 °C), their reduction temperatures were lower than those of the Mn_4Ce_1/cordierite catalyst, which indicated that the surface oxygen of ceria can be easily reduced.

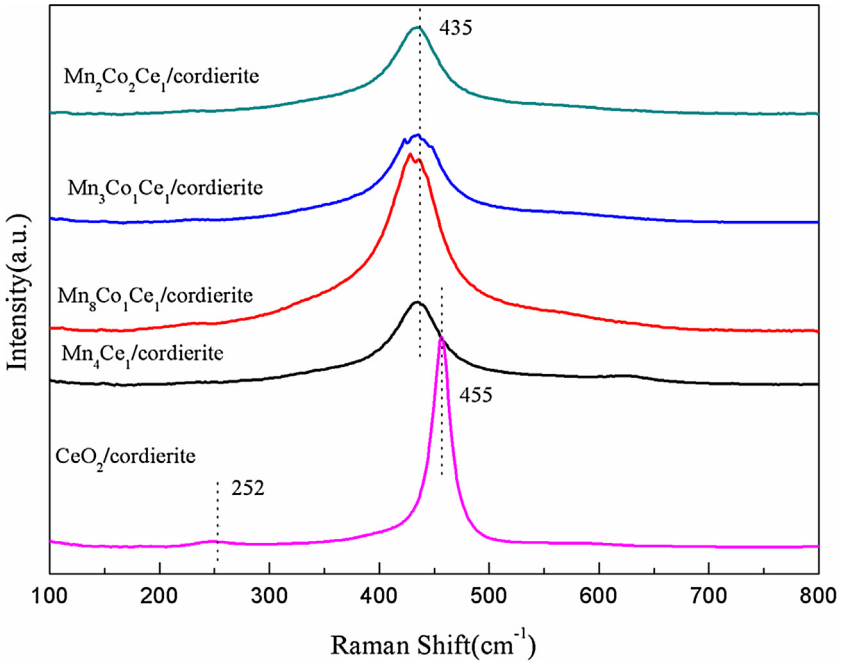

Fig. 5. Raman spectra of the synthesized catalysts (CeO_2/cordierite, Mn_4Ce_1/cordierite, and Mn-Co-Ce/cordierite).

However, the former present the Co_3O_4 phase: the reduction temperature and peak shape at 330 °C [47,48], which indicates that excessive cobalt ions can significantly change the structure of manganese and hinder the contact between CB and the active phase. Although the content of manganese is the same as that in the Mn_4Ce_1/cordierite catalyst, the reduction temperature of Mn_2O_3 in the $Mn_8Co_1Ce_1$/cordierite catalyst shifted to the left by approximately 24 °C. In addition, the reduction of the surface oxygen of ceria occurred at a higher temperature due to the decrease of a small amount of ceria or the strong interaction between CeO_2 and the manganese species [49,50]. It can be speculated that the addition of small amounts of cobalt ions promotes the incorporation of manganese into the CeO_2 lattice and changes the structure/phase of the manganese oxides, which can improve the mobility of active oxygen species on the surface, as active oxygen species are easily adsorbed on chlorobenzene and released to the reaction system by the synergistic effect of ceria, manganese and cobalt with variable valence states.

3.9. XPS characterization

To investigate the surface states and composition of the Mn_4Ce_1/cordierite and $Mn_8Co_1Ce_1$/cordierite catalysts, Fig. 7 shows XPS spectra of the O 1s, Mn 2p, Co 2p, and Ce 3d electronic levels in the catalysts above. The experimental and fitted Ce 3d spectra of the synthesized catalysts are shown in Fig. 7(A). Four

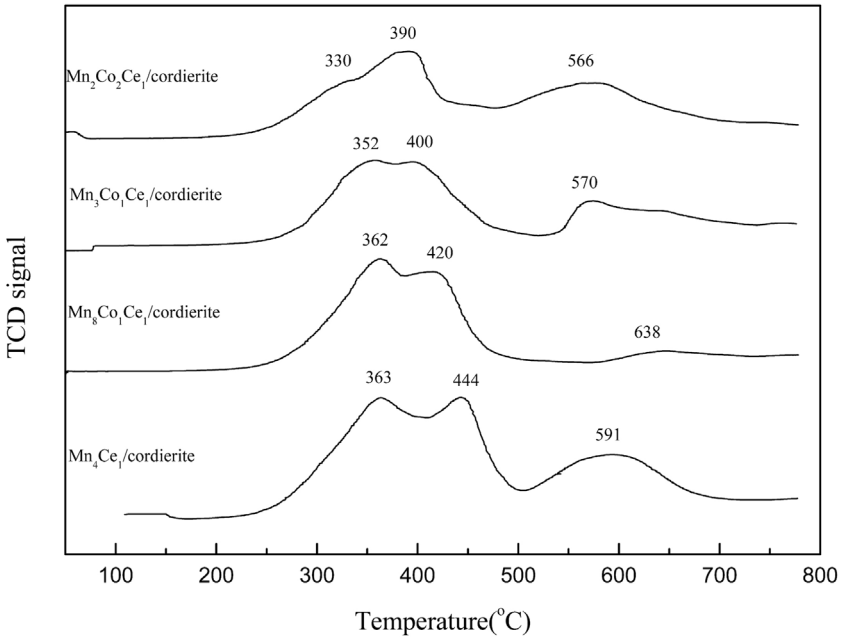

Fig. 6. TPR profiles of the Mn-Co-Ce/cordierite catalysts and the Mn_4Ce_1/cordierite catalyst.

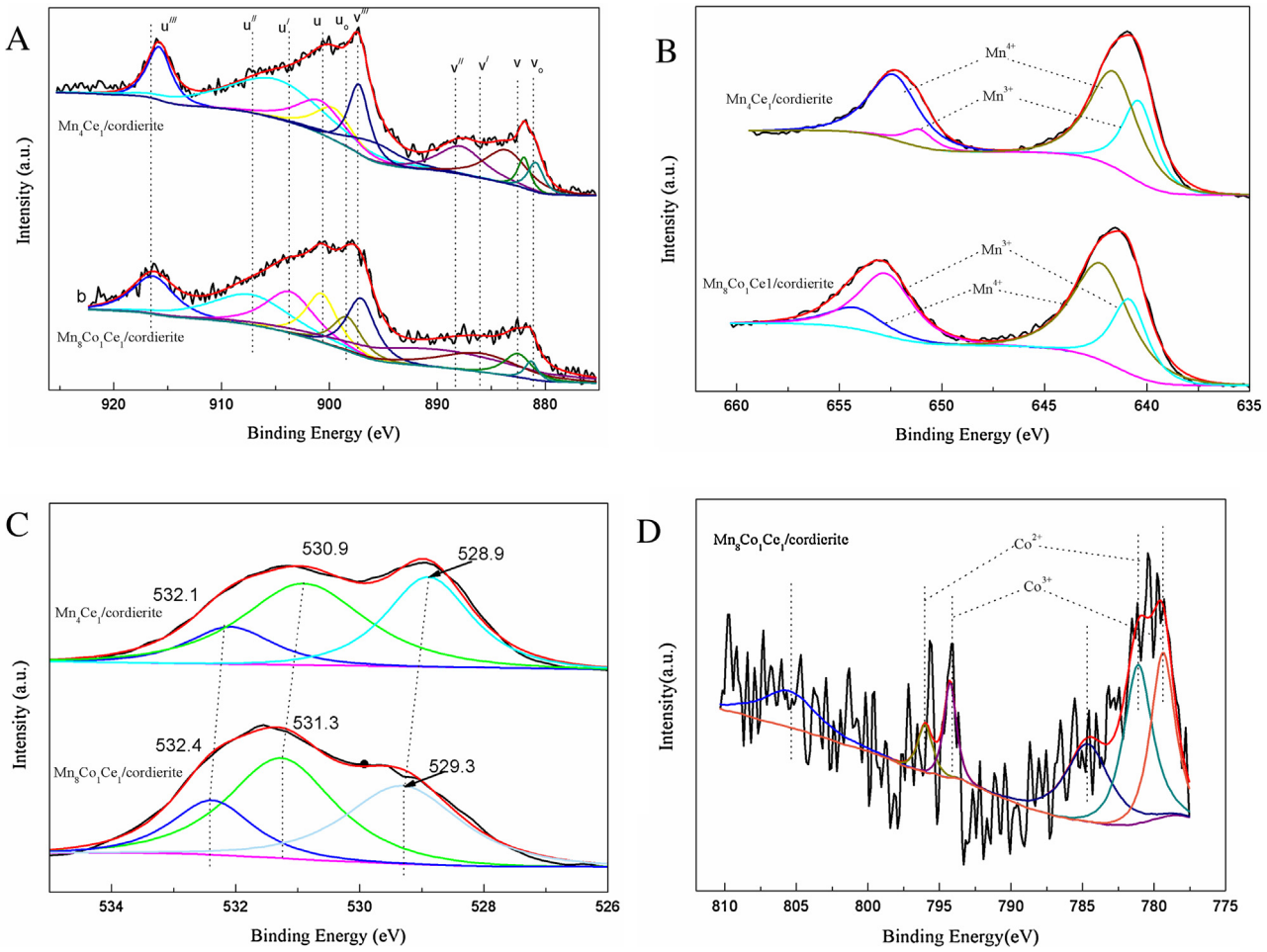

Fig. 7. XPS spectra of Ce 3d(A), Mn 2p(B), O 1s(C), and Co 2p(D) for the Mn4Ce/cordierite and Mn8Co1Ce1/cordierite catalysts.

peaks denoted as u', u_o, v', and v_o arise from the Ce^{3+} contribution, while Ce^{4+} is characterized by six other peaks. The existence of Ce^{3+} in the Mn_4Ce_1/cordierite and $Mn_8Co_1Ce_1$/cordierite catalysts indicates the formation of an oxygen vacancy, which can boost the oxygen transfer rate during chlorobenzene oxidation [51,52]. The fraction of Ce^{3+} ions with respect to the total cerium of the Mn_4Ce_1/cordierite and $Mn_8Co_1Ce_1$/cordierite catalysts is calculated as 17.8% and 20.7%, respectively, according to the measurement of the peak areas. Apparently, the peaks of the Ce^{3+} and Ce^{4+} ions experience some changes in their position and intensity upon cobalt doping, which can be attributed to the mixing with the Co 2p band [53,54]. The reducibility of ceria does not diminish the fraction of Ce^{3+} ions that are already present because the additional electrons in Ce^{3+} occupy localized cerium f-states that do not interact with each other. Fig. 7(B) shows the XPS spectra of Mn 2p. The binding energies of Mn $2p_{3/2}$ and Mn $2p_{1/2}$ are similar to those reported in the literature [55]. The component in the Mn_4Ce_1/cordierite at BE = 651.6 and 640.7 eV is attributed to Mn^{3+}, and that at BE = 653.1 and 642.1 eV is attributed to Mn^{4+} ions. On the other hand, the component in the $Mn_8Co_1Ce_1$/cordierite at 652.7 and 641.1 eV is assigned to Mn^{3+}, and that at BE = 654.1 and 642.4 eV is assigned to Mn^{4+} ions. When cobalt ions are mixed into the Mn-Ce/cordierite catalyst, the Mn^{4+}/Mn^{3+} ratio clearly decreases. It is speculated that more oxygen vacancies and lattice defects are formed by the addition of cobalt ions.

The O 1s XPS spectra for the Mn_4Ce_1/cordierite and $Mn_8Co_1Ce_1$/cordierite catalysts are deconvoluted into three contributions, as observed in Fig. 7(C). The binding energy (BE) at ca. 528.9–529.3 is assigned to the lattice oxygen (O^{2-}, denoted as O_α), and the binding energies at ~530.9–531.3 and ~532.1–532.4 are attributed to surface-adsorbed oxygen (O_2^-, O_2^{2-} or O^- denoted as O_β) and chemisorbed water, and dissociated oxygen and hydroxyl species (O_γ) [56]. Compared to the Mn_4Ce_1/cordierite catalyst, the binding energy of O_α over $Mn_8Co_1Ce_1$/cordierite increases due to the "Co ⟵ O" electron-transfer process, which indicates that the Co-doped Mn-Ce/cordierite promotes the formation of a ternary solid solution. Additionally, the concentration of O_β clearly increases from 48% to 60% (estimated through the integration of the peak areas), indicating that the catalytic activity can be improved and the Cl adsorbed on the surface of the catalysts can be removed quickly due to the higher mobility of O_β compared to that of O_α. Therefore, the addition of small amounts of cobalt ions to Mn-Ce/cordierite plays an important role in improving the catalytic activity and Cl resistance.

The Co 2p XPS spectra for the $Mn_8Co_1Ce_1$/cordierite samples are shown in Fig. 7(D). The original spectra are very disordered due to the low content of cobalt and interference of other species. The Co 2p spectra present two spin-orbit doublets and two shake-up satellite peaks. The binding energies at ca.779.6–781.3 and ca.794.3–795.9 are assigned to the two spin-orbit doublets, which can be attributed to Co $2p_{3/2}$ and Co $2p_{1/2}$; the other peaks are assigned to the satellite peak [57,58]. The Co $2p_{3/2}$ is deconvoluted into two components at BE = 779.6 and 781.3 eV; the former is attributed to the Co^{3+} species, whereas the latter is attributed to the Co^{2+} species. The Co $2p_{1/2}$ peak is also deconvoluted into two

components at BE = 794.3 and 795.9 eV, which correspond to the Co^{3+} and Co^{2+} species, respectively.

4. Conclusions

In this work, Mn-Ce/cordierite and Mn-Co-Ce/cordierite catalysts with different molar ratios were prepared by the sol-gel method and used in the catalytic combustion of low concentration chlorobenzene. Through characterization analysis by XRD, SEM, BET, H_2-TPR, Raman, and XPS, all catalysts presented morphological structures that are ball-like nanoclusters with asymmetrical sizes. A significant amount of manganese and small amounts of cobalt ions were incorporated into the lattice of ceria, which resulted in the formation of crystal defects and an improvement in the mobility of active oxygen species on the surface. The $Mn_8Co_1Ce_1$/cordierite catalyst presented a higher activity and stability than the other catalysts, and at least 90% chlorobenzene can be removed at 325 °C; in addition, the catalytic efficiency remained almost unchanged during a sustained reaction for 24 h at 350 °C. That high performance was ascribed to the synergistic effect of ceria, manganese and cobalt with variable valence states, which can promote the formation of more lattice defects and a smaller crystallite size. Moreover, the $Mn_8Co_1Ce_1$/cordierite catalyst should have a widespread application in the catalytic combustion of chlorinated volatile organic compounds.

Acknowledgments

This research is financially supported by the Project of Science and Technology Department of Jiangsu Province (BE2016769), the Natural Science Foundation of China (No. 51172107), the Natural Science Foundation of the Jiangsu Higher Education Institutions of China (No. 14KJB430014), the Open fund by Jiangsu Engineering Technology Research Center of Environmental Cleaning Materials (KFK1503) and A Project Funded by the Priority Academic Program Development of Jiangsu Higher Education Institutions (PAPD).

References

[1] P. Yang, S. Yang, Z. Shi, Z. Meng, R. Zhou, Appl. Catal. B: Environ. 162 (2015) 227–235.
[2] A. Śrębowata, R. Baran, D. Łomot, D. Lisovytskiy, T. Onfroy, S. Dzwigaj, Appl. Catal. B: Environ. 147 (2014) 208–220.
[3] H. Sedjame, C. Fontaine, G. Lafaye, J. Barbier Jr, Appl. Catal. B: Environ. 144 (2014) 233–242.
[4] A. Aznárez, R. Delaigle, P. Eloy, E.M. Gaigneaux, S.A. Korili, A. Gil, Catal. Today 246 (2015) 15–27.
[5] H. Huang, Y. Gu, J. Zhao, X. Wang, J. Catal. 326 (2015) 54–68.
[6] V.H. Vu, J. Belkouch, A. Ould-Dris, B. Taouk, J. Hazard. Mater. 169 (2009) 758–765.
[7] Q. Dai, S. Bai, J. Wang, M. Li, X. Wang, G. Lu, Appl. Catal. B: Environ. 142–143 (2013) 222–233.
[8] E. Finocchio, G. Ramis, G. Busca, Catal. Today 169 (2011) 3–9.
[9] J.M. Giraudon, A. Elhachimi, G. Leclercq, Appl. Catal. B: Environ. 84 (2008) 251–261.
[10] W. Deng, Q. Dai, Y. Lao, B. Shi, X. Wang, Appl. Catal. B: Environ. 181 (2016) 848–861.
[11] S. Zuo, M. Ding, J. Tong, L. Feng, C. Qi, Appl. Clay Sci. 105–106 (2015) 118–123.
[12] C. He, B. Xu, J. Shi, N. Qiao, Z. Hao, J. Zhao, Fuel Process. Technol. 130 (2015) 179–187.
[13] L. Zhang, S. Liu, G. Wang, J. Zhang, React. Kinet. Mech. Catal. 112 (2014) 249–265.
[14] Q. Dai, S. Bai, X. Wang, G. Lu, J. Porous Mater. 21 (2014) 1041–1049.
[15] M. Taralunga, J. Mijoin, P. Magnoux, Appl. Catal. B: Environ. 60 (2005) 163–171.
[16] W. Xingyi, K. Qian, L. Dao, Appl. Catal. B: Environ. 86 (2009) 166–175.
[17] P. Topka, R. Delaigle, L. Kaluža, E.M. Gaigneaux, Catal. Today 253 (2015) 172–177.
[18] S. Cao, H. Wang, F. Yu, M. Shi, S. Chen, X. Weng, Y. Liu, Z. Wu, J. Colloid Interface Sci. 463 (2016) 233–241.
[19] H. Huang, Q. Dai, X. Wang, Appl. Catal. B: Environ. 158–159 (2014) 96–105.
[20] C. He, Y. Yu, J. Shi, Q. Shen, J. Chen, H. Liu, Mater. Chem. Phys. 157 (2015) 87–100.
[21] X. Wang, Q. Kang, D. Li, Catal. Commun. 9 (2008) 2158–2162.
[22] P. Yang, Z. Shi, S. Yang, R. Zhou, Chem. Eng. Sci. 126 (2015) 361–369.
[23] H. Chen, H. Zhang, Y. Yan, Chem. Eng. Sci. 111 (2014) 313–323.
[24] D.M. Gómez, V.V. Galvita, J.M. Gatica, H. Vidal, G.B. Marin, Phys. Chem. Chem. Phys. 16 (2014) 11447.
[25] C. He, Y. Yu, Q. Shen, J. Chen, N. Qiao, Appl. Surf. Sci. 297 (2014) 59–69.
[26] Q. Huang, Z. Zhang, Y. Chen, S. Zhu, S. Shen, J. Chem. Eng. Jpn. 43 (2010) 413–420.
[27] Q. Dai, S. Bai, X. Wang, G. Lu, Appl. Catal. B: Environ. 129 (2013) 580–588.
[28] J.R. Gonzalez-Velasco, A. Aranzabal, R. Lopez-Fonseca, R. Ferret, J.A. Gonzalez-Marcos, Appl. Catal. B: Environ. 24 (2000) 33–43.
[29] R. Lopez-Fonseca, A. Aranzabal, J.I. Gutierrez-Ortiz, J.I. Alvarez-Uriarte, J.R. Gonzalez-Velasco, Appl. Catal. B: Environ. 30 (2001) 303–313.
[30] C.W.F.H. Pei Zhao, RSC Adv. (2014) 45665–45672.
[31] X. Ma, X. Feng, X. He, H. Guo, L. Lv, J. Guo, H. Cao, T. Zhou, Micropor. Mesopor. Mater. 158 (2012) 214–218.
[32] M. Wu, X. Wang, Q. Dai, D. Li, Catal. Commun. 11 (2010) 1022–1025.
[33] P.J. Jodłowski, R.J. Jędrzejczyk, A. Rogulska, A. Wach, P. Kuśtrowski, M. Sitarz, T. Łojewski, A. Kołodziej, J. Łojewska, Spectrochim. Acta Part A 131 (2014) 696–701.
[34] J. Chen, W. Shi, J. Li, Catal. Today 175 (2011) 216–222.
[35] J. Cheng, H. Wang, Z. Hao, S. Wang, Catal. Commun. 9 (2008) 690–695.
[36] P. Sun, W. Wang, X. Dai, X. Weng, Z. Wu, Appl. Catal. B: Environ. 198 (2016) 389–397.
[37] J. Lichtenberger, M.D. Amiridis, J. Catal. 223 (2004) 296–308.
[38] X. Wang, L. Ran, Y. Dai, Y. Lu, Q. Dai, J. Colloid Interface Sci. 426 (2014) 324–332.
[39] J. Li, P. Zhao, S. Liu, Appl. Catal. A: Gen. 482 (2014) 363–369.
[40] R. Ma, P. Hu, L. Jin, Y. Wang, J. Lu, M. Luo, Catal. Today 175 (2011) 598–602.
[41] Y. She, Q. Zheng, L. Li, Y. Zhan, C. Chen, Y. Zheng, X. Lin, Int. J. Hydrogen Energ. 34 (2009) 8929–8936.
[42] W.H. Weber, K.C. Hass, J.R. Mcbride, Phys. Rev. B 48 (1993) 178–185.
[43] A. Gurbani, J.L. Ayastuy, M.P. Gonzalez-Marcos, M.A. Gutierrez-Ortiz, Int. J. Hydrogen Energ. 35 (2010) 11582–11590.
[44] J. Trawczyński, B. Bielak, W. Miśta, Appl. Catal. B: Environ. 55 (2005) 277–285.
[45] B. Li, Q. Huang, X.K. Yan, X.L. Xu, Y. Qiu, B. Yang, Y.W. Chen, S.M. Zhu, S.B. Shen, J. Ind. Eng. Chem. 20 (2014) 2359–2363.
[46] X. Tang, Y. Xu, W. Shen, Chem. Eng. J. 144 (2008) 175–180.
[47] T. Cai, H. Huang, W. Deng, Q. Dai, W. Liu, X. Wang, Appl. Catal. B: Environ. 166–167 (2015) 393–405.
[48] M.H. Kim, K. Choo, Catal. Commun. 8 (2007) 462–466.
[49] J.L. Ayastuy, E. Fernández-Puertas, M.P. González-Marcos, M.A. Gutiérrez-Ortiz, Int. J. Hydrogen Energy 37 (2012) 7385–7397.
[50] P. Zhao, C. Wang, F. He, S. Liu, RSC Adv. 4 (2014) 45665–45672.
[51] C. He, Y. Yu, L. Yue, N. Qiao, J.I.L.Q. Shen, W. Yu, J. Chen, Z. Hao, Appl. Catal. B: Environ. 147 (2014) 156–166.
[52] J. Gonzalez-Prior, R. Lopez-Fonseca, J.I. Gutierrez-Ortiz, B. de Rivas, Appl. Catal. B: Environ. 199 (2016) 384–393.
[53] C. Gionco, M.C. Paganini, S. Agnoli, A.E. Reeder, E. Giamello, J. Mater. Chem. A 1 (2013) 10918–10926.
[54] W. Deng, Q. Dai, Y. Lao, B. Shi, X. Wang, Appl. Catal. B: Environ. 181 (2016) 848–861.
[55] Y. Zhang-Steenwinkel, J. Beckers, A. Bliek, Appl. Catal. A: Gen. 235 (2002) 79–92.
[56] C. He, X. Liu, J. Shi, C. Ma, H. Pan, G. Li, J. Colloid Interface Sci. 454 (2015) 216–225.
[57] J. Gonzalez-Prior, R. Lopez-Fonseca, J.I. Gutierrez-Ortiz, B. de Rivas, Appl. Catal. B: Environ. 199 (2016) 384–393.
[58] T. Cai, H. Huang, W. Deng, Q. Dai, W. Liu, X. Wang, Appl. Catal. B: Environ. 166 (2015) 393–405.